Available online at www.sciencedirect.com
SCIENCE DIRECT®
Continental Shelf Research 24 (2004) 659–671
CONTINENTAL SHELF RESEARCH
www.elsevier.com/locate/csr

A 2.5D model for sand transport in a shallow sea: effect of Ekman veering

G.I. Shapiro*,[1]

School of Earth, Ocean and Environmental Sciences, University of Plymouth, Drake Circus, Plymouth, Devon PL4 8AA, UK

Received 16 December 2002; received in revised form 5 December 2003; accepted 16 January 2004

Abstract

A process-based sediment transport model is presented that combines the knowledge of sediment transport in rivers and estuaries with the understanding of physical processes specific for the shelf seas. Due to formation of bottom Ekman spiral, the near-bottom current and hence the sediment transport deviate from the direction of surface current. The model takes into account velocity veering induced by Ekman spiral and estimates both direction and rate of transport of suspended particulate matter (SPM) generated by a steady or slowly varying current, through suspension, relocation and deposition of sediment in a shallow sea. The model uses a combination of analytical and numerical methods: analytical integration, in the vertical, and numerical integration, in the horizontal. The model predicts also vertical erosion/deposition fluxes at the seabed. The deviation angles and other parameters of SPM transport are computed for a range of water depths 5–50 m, particle settling velocities 0.1–6 cm/s, and current speeds 0.4–1.2 m/s. The model converges automatically to traditional engineering-style formulations, in extreme case of strong current in very shallow water, where velocity veering is of minor importance.

Keywords: Sediment transport; Boundary layer; Ekman spiral; Model; Shelf seas

1. Introduction

Most formulations for sediment transport were developed originally for rivers (Dyer, 1986; van Rijn, 1993). However, it is common practice to use these formulations for the marine environment, including tidally influenced areas, in a quasi-steady fashion (Soulsby, 1997; van der Molen, 2002; Calvete et al., 2001); this is despite the fact they are known to be less appropriate for use in the sea due to lack of specific marine physics. As a result, the accuracy of traditional sediment transport models in the marine environment is no better than the factor of 5, whilst in rivers the best formulae give predictions within a factor of 2 of the observed value (Soulsby, 1997). This paper presents a new sediment transport model that combines the knowledge of sediment transport in rivers and estuaries with an understanding of physical processes specific for shelf seas. The aim of the model is to estimate transport of suspended particulate matter (SPM) generated by a steady or slowly varying current, through suspension,

*Tel.: +44-1752-232406; fax: +44-1752-232406.
E-mail address: g.shapiro@plymouth.ac.uk (G.I. Shapiro).
[1]Also at P.P. Shirshov Institute of Oceanology, Moscow 117851, Russia.

0278-4343/$ - see front matter © 2004 Elsevier Ltd. All rights reserved.
doi:10.1016/j.csr.2004.01.001

relocation and deposition of a non-cohesive sediment.

The general principle for the calculation of total horizontal SPM fluxes is to integrate vertical profiles of SPM concentration and current velocity, over the thickness of the nepheloid (sediment laden) layer, at each horizontal location (Dyer, 1986). In the SPM transport models, which have been developed for relatively shallow water pools (rivers, estuaries) it is common to adopt a logarithmic velocity distribution, (see e.g. Sleath, 1984). However, in the marine environment where the depth of water exceeds the Ekman scale, H_E, (typically 10–30 m), shear stress changes with depth due to the Coriolis force, this mostly occurs above a relatively thin (about $0.1H_E$) logarithmic velocity sub-layer. This interaction results in the formation of a bottom Ekman spiral; hence, both speed and direction of the current change with depth (Csanady, 1982). In particular, the direction of the current, and thus, the direction of sediment transport near the seabed is different from that of the surface current. Qualitatively, it became clear as far back as in 1972 that velocity veering in the bottom Ekman layer under ocean currents might be an important mechanism of cross-shore SPM transport (McCave, 1972).

The present model incorporates the effect of velocity veering due to Ekman spiral into advection–diffusion balance of suspended material and computes SPM transport and erosion/deposition rates at sea floor by considering deviation of the SPM flux from the direction of surface current, see Fig 1. Velocity veering effects both cohesive and non-cohesive sediment transport. The model occupies a niche between 2DH models (see e.g. Schoonees and Theron, 1995 for overview) and fully 3D (e.g. Proctor et al., 2001; Davies and Xing, 2001, 2002) numerical models; as such it is called here a 2.5D velocity veering SPM (VVS) transport model. The advantage of the model is that it uses a combination of analytical and numerical methods: analytical integration in the vertical and numerical integration in the horizontal.

Solutions to the governing equations in the vertical direction are obtained using analytical methods, which is equivalent to employing an infinite number of numerical layers. However, as with all analytical methods, it is necessary to introduce some physical simplifications in order to derive a solution, in particular in terms of parameterization of turbulent diffusion. The parameterization used in this paper is similar to the classical Ekman spiral, which was shown to provide a good statistical fit to observed current velocities in the ocean (Stacey et al., 1986). The horizontal transport rates and the vertical fluxes (i.e. erosion/deposition rates) are computed numerically or analytically depending on the complexity of a particular problem. This approach allows to calculate the horizontal SPM transport for complex current patterns and over complex bottom topography. It also results in a numerical code for the model that is significantly faster than 3D models and can be used for quick transport estimates.

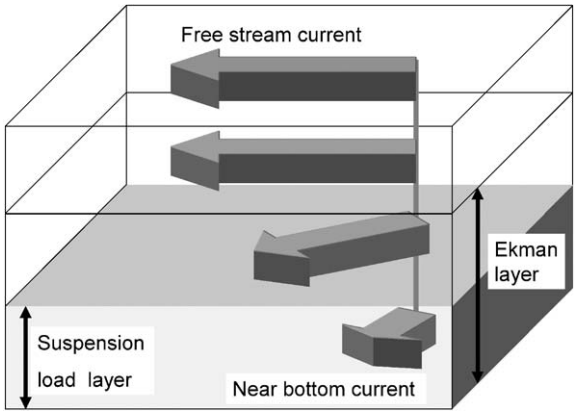

Fig. 1. Conceptual scheme of velocity veering and its influence upon suspended sediment transport. Suspended material typically occupies only the lower part of the Ekman layer where the direction of current is different from that of the free stream current. This results in the depth-integrated sediment transport being at an angle to the depth-integrated water flow.

2. Model description

The accuracy of the sediment transport models is not generally high (Soulsby, 1997), so it would be unrealistic to attempt development of a fluid dynamic model which could predict the sediment

transport rates or concentration of suspended sediment with the accuracy much better than a factor of 2. This is why the proposed model focuses upon the main physical effects and first-order estimates; it utilizes approximate methods of solving analytical equations; furthermore, it includes only two commonly used empirical (tuning) parameters.

The model follows arbitrary bottom topography, although there are the usual restrictions on the steepness of the slope (hydrostatic approximation). The main new aspect of the model is that it incorporates the effect of velocity veering in the bottom boundary layer of the sea and replaces the logarithmic velocity profile with a more appropriate approach to the marine environment, the Ekman spiral. A similar idea was used for the modelling of fine-grained cohesive sediment in response to mesoscale currents on the outer shelf and continental slope of the Black Sea (Shapiro et al., 2000). However, the new model is designed specifically to simulate transport in shallow seas, which may have a water depth comparable or smaller than the Ekman scale and uses a different turbulent closure scheme. Apart from non-cohesive sediment, the same algorithm can be used for modelling the cohesive sediment transport, the difference in physical properties being reflected in the form of the pick-up and deposition functions, which should be specified by the user as described below in Section 2.

In designing the model, we distinguish two boundary layers: (1) the Ekman layer, where velocity veering, generation of shear stress and turbulent mixing takes place; and (2) the nepheloid layer, where the SPM is concentrated, see Fig 1. The thickness of the Ekman layer depends upon the hydrodynamics of the water flow, but not on the presence of the sediment, as we consider relatively small SPM concentrations, which are typical for the shelf seas (McCandliss et al., 2002) and ignore the effect of damping turbulence by high concentrations of sediment (Barenblatt and Golitsin, 1973). The thickness of the nepheloid (suspension load) layer is controlled by the balance of turbulent lift versus gravitational settling, which is calculated within the model and depends upon parameters of both the flow and sediment; generally, these layers do not coincide. As the upward motion of sediment particles is due to turbulent eddies and, in the absence of waves and wind, the production of turbulence is confined within the Ekman layer, it is reasonable to expect that the bottom nepheloid layer could not extend higher than the Ekman layer.

The following simplifying assumptions are made in the mathematical formulation of the model: the flow is unstratified and steady (or varying with a subtidal rate) and there are no waves or wind; horizontal scales of motion are much greater than the vertical ones.

Within these approximations, the equations of motions are

$$-fv = -\frac{1}{\rho}\frac{\partial p}{\partial x} + \frac{\partial \tau_x}{\partial z}, \tag{1}$$

$$fu = -\frac{1}{\rho}\frac{\partial p}{\partial y} + \frac{\partial \tau_y}{\partial z}, \tag{2}$$

$$\tau_x = K_z \frac{\partial u}{\partial z}, \quad \tau_y = K_z \frac{\partial v}{\partial z}, \tag{3}$$

where u, v are the components of horizontal current velocity as functions of x, y, z, t; p is the pressure; f is the Coriolis parameter, ρ is the density, τ is the Reynolds shear stress per unit mass, and K_z is the turbulent friction coefficient.

Eqs. (1)–(2) are subject to the following boundary conditions: (i) no slip at the sea bed; (ii) no shear stress at the sea surface, (iii) a given current velocity at the sea surface; and (iv) a given shear stress at the seabed

$$u = u_h, \quad v = v_h \quad \text{at } z = h, \tag{4}$$

$$|\tau| = u_*^2 \quad \text{at } z = 0, \tag{5}$$

where z is the height above bottom. The values of friction velocity, u_*, surface velocity (u_h, v_h), and water depth, h, may vary in the horizontal. The use of a no-slip condition (e.g. Davies and Jones, 1990) implies that the model incorporates a near-bottom velocity profile, which is often approximated by a logarithmic function, as a lower part of the Ekman spiral.

The turbulent viscosity coefficient, K_z, is obtained using a simple turbulence closure scheme, which has been used successfully by a number of

authors. Csanady (1982) suggests that outside wall layers, but within a turbulent shear flow region, turbulent viscosity may be taken as constant. The numerical study of Lentz (1995) shows also that the along-shelf circulation on the shelf is not sensitive to the actual form of the turbulent viscosity profile. In the present study, the eddy viscosity K_z is assumed to have no vertical variations within the Ekman layer of a thickness of about $2H_E$, where H_E is the Ekman scale. Above the Ekman layer, the shearing stress and levels of turbulence are small, and the eddy viscosity K_z is taken as zero. This schematization does not lead to much error, as was shown by Rossby and Montgomery, who solved the equations with various likely vertical profiles of $K_z(z)$ and found only detailed differences from the Ekman's solution (cited via Pond and Pickard, 2001, Section 9.45). However, the eddy viscosity K_z may vary in the horizontal, due to changes in u_* and H_E, and this effect is taken into account in the VVS model.

Eqs. (1)–(7) have an approximate analytical solution, which can be expressed conveniently in complex variables

$$S(z) = S_h \frac{\cosh(\lambda h)}{\cosh(\lambda h) - 1}\left(1 - \frac{\cosh[\lambda(h - z)]}{\cosh(\lambda h)}\right), \quad (6)$$

where $S = u + \mathrm{i}v$, $\mathrm{i} = \sqrt{-1}$, $\lambda = (1 + \mathrm{i})/H_E$, and the Ekman scale is

$$H_E = \sqrt{\frac{2K_z}{f}}. \quad (7)$$

Note that in civil engineering applications it is more common to use the depth-averaged, $\bar{S}$, rather than surface, S_h, velocity. In complex variables, the relationship between the two velocities is given by

$$\frac{\bar{S}}{S_h} = \frac{\cosh(\lambda h)}{\cosh(\lambda h) - 1}\left(1 - \frac{\mathrm{i}}{\lambda h}\frac{\sinh(\lambda h)}{\cosh(\lambda h)}\right). \quad (8)$$

The equation for the turbulent viscosity coefficient, K_z, is obtained by matching the shear stress at the seabed, from Eqs. (3) and (5).

$$u_*^2 = \tau|_{z=0} = K_z\left|\frac{\partial S}{\partial z}\right|_0 = K_z\left|\frac{\lambda S_h \sinh(\lambda h)}{\cosh(\lambda h) - 1}\right|. \quad (9)$$

In order to solve Eq. (9) we express the frictional velocity at the seabed, u_*, via the surface current, using the bulk formula

$$u_*^2 = C_D|\mathbf{u}_h|^2, \quad (10)$$

where C_D is the empirical drag coefficient due to current (Csanady, 1982). Note that Eq. (10) is sometimes used in relation to current at a specific reference level above bottom, which gives a different numerical value for C_D (e.g. Davies and Xing, 2002). The alternative values of C_D are easily cross-related using the velocity profile $u(z)$, derived from Eq. (6). An approximate analytical interpolating solution to the set of Eqs. (7), (9) and (10) is

$$K_z = \begin{cases} \dfrac{2C_D^2|\mathbf{u}_h|^2 h}{2fh + C_D|\mathbf{u}_h|} & \text{at } 0 < z < 2H_E, \\ 0 & \text{at } 2H_E < z. \end{cases} \quad (11)$$

This formula provides an explicit expression for the eddy viscosity, K_z, via the speed of the surface current, u_h, and depth of water, H. Eq. (6) provides vertical profiles of both magnitude and direction of the current in the bottom boundary layer. The near-bottom current is directed to the left (in the Northern Hemisphere) of the surface current, in agreement with the Ekman theory. The novelty compared to the standard Ekman spiral is that: (i) the eddy viscosity, thickness of the Ekman layer and parameters of the spiral are not prescribed constants, but are dependent on the strength of the surface current according to Eq. (11); and (ii) parameters of the spiral may vary in the horizontal. The only tuning parameter used in the model is the drag coefficient C_D, which is usually estimated from hydraulic experiments, current observations, see e.g. Ramp and Abbott (1998), or bed roughness measurements.

The strength of the veering can be estimated as the angle, α, between the surface current and the bottom shear stress. Simple manipulations with Eqs. (6) show that

$$\alpha = \arg\left(\frac{(1 + \mathrm{i})\sinh(\lambda h)}{\cosh(\lambda h) - 1}\right) \quad (12)$$

and the veering angle is confined within the range of approximately 0–45°. The direction of the near-bottom current does not necessarily coincide with the direction of the net sediment flux, as the direction of current within the bottom nepheloid layer may change with depth. Since the bedload

transport, which is not the focus of this paper, is always in the direction of the bottom shear stress, Eq. (12) may be helpful in estimating impact of velocity veering on bedload transport.

The advection–diffusion equation for the SPM concentration is

$$\frac{\partial C}{\partial t}+\frac{\partial (uC)}{\partial x}+\frac{\partial (vC)}{\partial y}+\frac{\partial [(w-w_s)C]}{\partial z} = \frac{\partial}{\partial z}\left(K_c\frac{\partial C}{\partial z}\right), \quad (13)$$

where w_s is the settling velocity of suspended particles, and K_c is the turbulent diffusion coefficient. Within the SPM cloud, the concentration gradients are often much larger in the vertical, than in the horizontal. In such circumstances, the first three terms (phase lag, horizontal advection) of Eq. (13) are smaller than the last two terms (gravitational fall of particles and their upward motion due to turbulence). This is why single-point 1D models, which utilize only these two terms, often produce reasonable estimates of SPM concentration (McCandliss et al., 2002), although in some circumstances horizontal advection can be important (e.g. Davies and Xing, 2002; Bass et al., 2002). This is particularly the case when velocity veering is considered and the effect of horizontal advection is incorporated into the VVS model.

Eq. (13) is often used in a depth-integrated form (e.g. Bass et al., 2002)

$$\frac{\partial h\bar{C}}{\partial t}+\frac{\partial}{\partial x}h(\overline{uC})+\frac{\partial}{\partial y}h(\overline{vC})=E_r-D, \quad (13a)$$

where $h\bar{C}$ is the depth-integrated concentration (the suspended load), $h(\overline{uC})$, $h(\overline{vC})$ are the depth-integrated horizontal SPM transport rates. The terms on the right-hand side are the sources and sinks of sediment to the system, E_r is the rate of erosion and D is the rate of deposition. For cohesive sediment, the specific expressions of E and D are discussed in a number of papers (e.g. Teisson, 1997). For non-cohesive sediment, these expressions can be determined from more commonly used "reference concentration" formulations as shown below in Section 3.1.2. Further derivation is not based upon any particular expression for the pick-up and deposition functions, which should be specified by the user of the model.

The non-local effects, i.e. advection, and the phase lag between erosion and deposition of material are treated as follows. Eq. (13) is solved using an iterative procedure, which employs a single–point model, as a zero-order approximation. A reduced, single-point version of Eq. (13) is

$$-w_sC=K_c\frac{\partial C}{\partial z}, \quad (14)$$

where the vertical velocity of water, w, is neglected compared to the settling velocity, and no vertical sediment flux assumed at the sea surface.

Solution to Eq. (14) gives the vertical profile of SPM concentration

$$C(z)=C_0\exp\left(-\int_0^z\frac{w_s\,\mathrm{d}z}{K_c}\right). \quad (15)$$

Correct parameterization of the diffusion coefficient can have significant influence on sediment balance (e.g. Davies and Xing, 2002). Direct numerical simulations of the turbulent Ekman layer showed that turbulent kinetic energy (and hence eddy diffusion and viscosity) is mostly concentrated in a near-bottom layer (Coleman et al., 1990). The thickness of this layer, typically $(0.1-0.25)u_*/f$, is equivalent to a few Ekman depths (for details see Section 3 below). In the VVS model the vertical variation of eddy diffusion is approximated by a piecewise function, i.e. K_c has a constant value equal to the eddy viscosity K_z, within the bottom layer of thickness $2H_E$ and drops to zero above it.

With this approximation for K_c, Eq. (15) for the vertical profile of SPM concentration reduces to

$$C(z)=C_0\beta(z). \quad (16)$$

Here, the non-dimensional concentration profile is given by

$$\beta(z)=\begin{cases}\exp(-z/h_d) & \text{at } 0<z<2H_E,\\ 0 & \text{at } 2H_E<z,\end{cases} \quad (17)$$

where

$$h_d=\frac{K_z}{w_s} \quad (18)$$

is the height of e-fold decrease of SPM concentration.

In contrast to a single-point theory, the value C_0 is left at this stage as an unknown function of time and horizontal co-ordinates rather than being obtained from local boundary conditions. Its value will be computed later from the non-local balance, which includes contribution from all the terms of Eq. (13). With C_0 still being an unknown parameter, Eq. (16) does not give the absolute value of concentration; however, it fixes the non-dimensional shape of the profile. Similar analytical methods have been used in chemical technology (Alekseenko et al., 1992), shallow water dynamics (Xu, 1995), and in simulation of sediment transport by eddies (Shapiro et al., 2000). In contrast to the VVS, the latter model uses a 'constant value' rather than piecewise approximation for the diffusion coefficient and is only valid for deep waters ($h \gg H_E$).

If $h_d < 2H_E$ then h_d represents the thickness of the bottom nepheloid layer, h_c. If $h_d > 2H_E$, which may happen for small values of settling velocities, w_s, or high level of turbulence (large K_z), then the concentration profile is more uniform within the Ekman layer. The concentration diminishes sharply above the bottom mixed layer, as there are no local sources of turbulence. In this case, the thickness of the nepheloid layer is given by $2H_E$. Generally,

$$h_c = \min(h_d,\ 2H_E,\ h). \tag{19}$$

It is useful to relate the unknown value of near bottom SPM concentration C_0 to another yet unknown value, the total suspension load, m, i.e. total mass of SPM over a unit area of seabed

$$m = \int_0^h C(z)\,\mathrm{d}z = h\bar{C}. \tag{20}$$

Substitution of Eq. (16) into Eq. (20) yields the relationship

$$m = \gamma C_0 h_d, \tag{21}$$

where the SPM load form-factor, γ, is

$$\gamma = \begin{cases} \left[1 - \exp\left(-\dfrac{h}{h_d}\right)\right] & \text{at } h < 2H_E. \\ \left[1 - \exp\left(-\dfrac{2H_E}{h_d}\right)\right] & \text{at } 2H_E < h. \end{cases} \tag{22}$$

The integral version of the SPM advection–diffusion equation (13a) can now be re-written in the form

$$\frac{\partial m}{\partial t} + \frac{\partial Q_x}{\partial x} + \frac{\partial Q_y}{\partial y} = E - \frac{w_s m}{h_d \gamma}, \tag{23}$$

where $Q_x = h\overline{Cu}$ ($Q_y = h\overline{Cv}$) is the depth-integrated SPM transport in the x (y) direction, and $E = E_r - D'$ is the full entrainment (sediment 'pick-up') function, which depends upon both parameters of the water flow and condition of bottom sediment. The term D' represents the correction to the gravitational deposition rate, $w_s C_0$, and relates to the critical deposition shear stress below which material will settle to the bed (e.g. Teisson, 1997). This term is only important for cohesive sediment. By now we have expressed the near-bottom concentration via the SPM load using Eqs. (21) and (22). In order to obtain a closed equation for SPM load we need to express SPM transport rates Q_x and Q_y in terms of SPM load and parameters of the flow. This is done through an iterative procedure, as described below.

From Eq. (23) we obtain the first-order equation for m by calculating horizontal SPM fluxes using the non-dimensional concentration profile from Eq. (17) as a zero-order approximation. Using complex variables, we introduce a zero-order SPM mass transport rate, Q, as follows:

$$\begin{aligned} Q = Q_x + \mathrm{i}Q_y &= \int_0^h S(z)C(z)\,\mathrm{d}z \\ &= S_h m \Omega(x,\ y), \end{aligned} \tag{24}$$

where the concentration profile is given by Eq. (16), the relationship between C_0 and the SPM load is given by Eq. (21), and the (complex) velocity veering function, Ω, is introduced as follows:

$$\begin{aligned} \Omega(x,\ y) = &\frac{1}{h_d \gamma}\frac{\cosh(\lambda h)}{\cosh(\lambda h) - 1} \\ &\times \int_0^h \left(1 - \frac{\cosh(\lambda(h - z))}{\cosh(\lambda h)}\right)\beta(z)\,\mathrm{d}z, \end{aligned} \tag{25}$$

where the SPM form-factor, γ, is given by Eq. (22). Substitution of Eqs (22) into (25) yields

$$\Omega(x,\ y) = \frac{\cosh(\lambda h)}{\cosh(\lambda h) - 1} \times \left[1 - \frac{e^{\lambda h} G_+ + e^{-\lambda h} G_-}{2\gamma \cosh(\lambda h)}\right], \quad (26)$$

where

$$G_+ = \frac{1 - \exp\left(-[(1 + \lambda h_d)\sigma]/h_d\right)}{1 + \lambda h_d},$$

$$G_- = \frac{1 - \exp\left(-[(1 - \lambda h_d)\sigma]/h_d\right)}{1 - \lambda h_d},$$

$$\sigma = \min(h,\ 2H_E). \quad (27)$$

The dimensionless function Ω shows how the actual SPM transport rate differs from a simple product of the SPM load by the surface current. The imaginary part of Ω reflects the deviation of the net SPM transport from the direction of the current.

Now all the SPM parameters are expressed in terms of total SPM load, m, so that the SPM transport equation (23) is closed and can be solved using numerical methods. Eq. (23) is only in 2D and, hence, is much simpler to solve than the original equation (13), as used in fully 3D models (e.g. Proctor et al., 2001; Davies and Xing, 2002). After Eq. (23) has been solved, a full 3D picture of SPM distribution, i.e. $C(x, y, z, t)$, is obtained from the 2D distribution of SPM load, $m(x, y, t)$, and explicit formulae (16), (17), (21) and (22). The integrals in Eq. (24) and (25) are calculated analytically, which simplifies the numerical solution of Eq. (23).

If necessary, further iterations can be formally performed. For example, the second-order equations are obtained by calculating corrections to the shape, $\beta(z)$, of the vertical SPM concentration profile from Eq. (13), where the first-order values of $C(x, y, z, t)$ are substituted into the first three terms of the equation, and the stages shown by Eqs. (20)–(24) are repeated. However, the main effect of velocity veering is already seen in the first-order equations (23) and (24) and any further iterations are unlikely to be necessary.

The morphological effect of SPM transport is controlled by the vertical SPM flux at the seabed, F_v, which is determined by the amount of eroded material minus the amount of deposited material, i.e. is given by the RHS of Eq. (23).

$$-\rho \frac{dZ_b}{dt} = F_v = E - D, \quad (28)$$

where

$$D = \frac{w_s m}{h_d \gamma} \quad (29)$$

is the gravitational downward flux and Z_b is the height of the sea bed above its initial level. It should be noted that a zero vertical SPM flux at the sea surface is assumed. In the zero-order (single-point) approximation the erosion/deposition flux, F_v, is obviously zero. The lowest-order approximation which gives a non-trivial result is the first-order equation (23).

For truly steady-state conditions, Eq. (23) can be further simplified and solved using expansion in small parameter, ε, which represents a typical ratio of the LHS of Eq. (23) and the entrainment (E) or deposition (D) fluxes, whichever is greater.

Let

$$m = m_0 + \varepsilon m_1 + \cdots, \quad F_v = F_{v0} + \varepsilon F_{v1} + \cdots.$$

By substituting this expansion set into Eq. (23) and equating the terms, which are proportional to ε^o, we have

$$m_0 = \frac{E h_d \gamma}{w_s},$$

$$F_{v0} = 0.$$

In the next order of ε we obtain a correction term to the depth-integrated SPM load,

$$\varepsilon m_1 = \frac{m_0}{E}\left[\frac{\partial(m_0 \mathrm{Re}(S_h \Omega))}{\partial x} + \frac{\partial(m_0 \mathrm{Im}(S_h \Omega))}{\partial y}\right]$$

and an analytical expression for the vertical flux, F_v, at the seabed

$$F_v = \varepsilon F_{v1} = \frac{\partial(m_0 \mathrm{Re}(S_h \Omega))}{\partial x} + \frac{\partial(m_0 \mathrm{Im}(S_h \Omega))}{\partial y}.$$

Here, the symbols Re and Im represent, respectively, the real and imaginary parts of the complex variable. Positive values of F_v relate to prevailing erosion, negative values represent predominance of deposition.

3. Results and discussion

Application of the model requires the following input information: (1) full depth of water as a function of horizontal co-ordinates $h(x,y)$; (2) surface currents $u_h(x,y)$, $v_h(x,y)$, (3) drag coefficient C_D or an equivalent parameter (e.g. bottom roughness); (4) settling velocity of suspended particles w_s; (5) sediment entrainment (pick-up) rate E, which can be a function of the location, sediment properties, bottom shear stress, etc; and (6) the Coriolis parameter. Another important factor, the availability of sediment on the seabed can be controlled by spatial and temporal variations in E, e.g. by setting $E=0$ if the source of bottom sediment is exhausted.

From the input parameters, the values of K_z, K_c, H_E and λ are calculated using Eqs. (11) and (7), then h_d and γ are obtained from Eqs. (18) and (22), and finally the function Ω is obtained from Eqs. (25)–(27). After substitution of these values into Eq. (23), this equation is solved numerically or analytically in respect to the SPM load, m, as discussed in the previous Section.

The output of the model includes: (1) the absolute value and direction of the SPM transport rate, Q; (2) the rate (vertical flux) of sediment erosion or deposition as a function of location; (3) thickness of the near-bottom nepheloid layer and a 3D distribution of SPM concentration. As a side product the model provides information about: (4) direction of the bottom shear stress to be used for calculation of bedload transport; (5) the surface SPM concentration.

The 'pick-up' function is arguably the less known parameter of sediment transport and is generally obtained as the 'best fit' to observations. However, the model allows calculating some of the characteristics of sediment transport, which are not sensitive to the exact value of the 'pick-up' function and can be more easily compared with other theories and observations. These characteristics are: (1) the eddy viscosity coefficient, K_z; (2) the angle of SPM veering, α_{SPM}; and (3) the thickness of the Ekman and nepheloid layers.

The angle of deviation of the SPM transport from the surface current, α_{SPM}, is calculated using the complex function Ω given by Eq. (25)

$$\alpha_{SPM} = \tan^{-1}\left(\frac{\Omega_i}{\Omega_r}\right), \tag{30}$$

where Ω_r (Ω_i) is the real (imaginary) part of Ω. Positive values of α_{SPM} correspond to left rotation (in the Northern Hemisphere) of SPM transport relative to the surface current.

3.1. Comparison with observations and existing theories

Whilst a detailed validation of the model would require a focused field programme, some of the model elements can be checked against existing theories and observations.

3.1.1. Flow regime

Let us consider the hydrodynamic properties of the model in extreme cases of very shallow ($h \ll H_E$) and very deep ($h \gg H_E$) waters.

At a *very shallow limit*, $h \ll H_E$, Eq. (11) reduces to

$$K_z = 0.5 C_D |\mathbf{u}_h| h = 0.5\sqrt{C_D} u_* h. \tag{31}$$

Eq. (31) is similar to the equation used by van Rijn (1993) for the description of turbulent flows without the Coriolis force. If we take $C_D = 4\kappa^2/\alpha_1^2$, where κ is the von Karman constant, α_1 is the empirical constant used by van Rijn, then our Eq. (31) becomes identical to van Rijn's equation (7.3.12). As expected, in very shallow waters the role of Coriolis force diminishes, and both veering angles, α, and α_{SPM} tend to zero as $h/H_{E^-} > 0$. Assuming the parameter h_d does not exceed the full water depth, the asymptotic expression for the thickness on the nepheloid layer becomes

$$h_c = \frac{\sqrt{C_D} u_* h}{2 w_s}.$$

This equation is consistent with Eq. (7.3.18) of van Rijn, if the empirical coefficient C_D is tuned as follows:

$$C_D = \frac{4\beta_e^2 \kappa^2}{\alpha_1^2},$$

where β_e is the empirical beta-factor, see van Rijn (1993, Eq. 7.3.16).

In *deep waters*, i.e. at bottom depths $h \gg 2H_E$, the expression for the viscosity coefficient reduces to the formula obtained by Shapiro et al. (2000), for the deep water limit:

$$K_z = \frac{u_*^4}{f|S_h|^2} = \frac{C_D^2|\mathbf{u}_h|^2}{f}. \quad (32)$$

Eq. (32) can be re-written in the form

$$H_E = \sqrt{2C_D}\frac{u_*}{f}, \quad (33)$$

which has the same functional dependence of u_* and f as the equation for the Ekman scale introduced by Csanady (1982, Section 6.2.3). Numerical coefficient recommended by Csanady is 0.1, and our Eq. (33) coincides exactly with Eq. (1.52) by Csanady if $C_D = 5 \times 10^{-3}$. Numerical coefficient given in Simpson (1998) corresponds to $C_D = 2 \times 10^{-3}$. Both Eqs. (31) and (32) are consistent with the length-of-mixing theory (Monin and Yaglom, 1971). Eq. (32) is similar to that of Davies and Jones (1990).

There are a few observational studies that can be compared qualitatively with the VVS model output. Firstly, observational evidence of bottom Ekman spiral has been reported extensively in the literature. More specifically, the rotation of currents with depth near the seabed in relatively shallow water has been presented in a number of publications, e.g. Niedoroda and Swift (1991), Ramp and Abbott (1998). The model shows clearly such behaviour over a range of current speeds, if the water depth is greater than about 5–10 m. Secondly, the model provides reasonable estimates of the turbulent viscosity coefficient and thickness of the bottom Ekman (mixed) layer. Measurements by Lentz and Trowbridge (1991) show that bottom mixed-layer heights are typically 5–15 m but, occasionally, exceed 50 m. Observations obtained from the continental shelf off northwest Africa have revealed that the bottom Ekman layer is about 25 m thick (Tomczak and Hao, 1989) These values are consistent with the results obtained with the VVS model, Eq. (11).

The analysis presented above shows that the hydraulic component of the VVS model is consistent with observations and reduces to existing theories, in extreme cases.

3.1.2. Transport rates

The SPM transport rates and concentration profiles as given by the VVS model are compared, in this Section, with: (i) observations taken in a relatively shallow flow (no velocity veering); and (ii) some frequently used sand transport formulations, which ignore the Coriolis effect. The following calculations follow mainly the Example (7.4.3) of van Rijn (1993), where details of measurements and comparison with Bagnold, Smith-McLean and van Rijn theories are given. The measurements were carried out in the Mississippi River in April 1961. The water depth was $H = 12.05$ m, mean velocity $\bar{u} = 1.55$ m/s; the bed material characteristics were $d_{35} = 350$ mkm, $d_{50} = 400$ mkm, $d_{90} = 1500$ mkm, sediment density $\rho = 2650$ kg/m^3; the measured suspended load transport was $Q = 2.4$ kg/sm; the seabed roughness was determined as $z_0 = 0.007$ m; and the settling velocity, based upon d_{50} grain size, was $w_s = 0.059$ m/s.

The SPM transport rates calculated using the VVS model over a range of flow velocities, are compared in Fig. 2, with observational data and computations made according to the methods of van Rijn (simplified formulation), Bagnold, and Bailard; see e.g. Eqs. (7.3.46) and (7.3.40) in van Rijn (1993), and Eq. (134d) in Soulsby (1997). The following empirical parameters were used as recommended by van Rijn and Soulsby: for the Bagnold method—$e_b = 0.1$, $e_s = 0.02$; and for the Bailard method—$\varepsilon = 0.02$. Eq. (7.3.46) of van Rijn does not have any tuning parameters within a velocity range of 0.5–2.5 m/s. The parameters in the VVS model were selected as follows. Drag coefficient is related to the seabed roughness, z_0, through a standard expression

$$C_D = \frac{\kappa^2}{\ln^2(H/z_0)}. \quad (34)$$

The calculation of the pick-up function, E, is based upon an energy concept. Its value is computed by equating the SPM load, m, from a single-point version of Eq. (23)

$$m = \frac{Eh_d\gamma}{w_s} \quad (35)$$

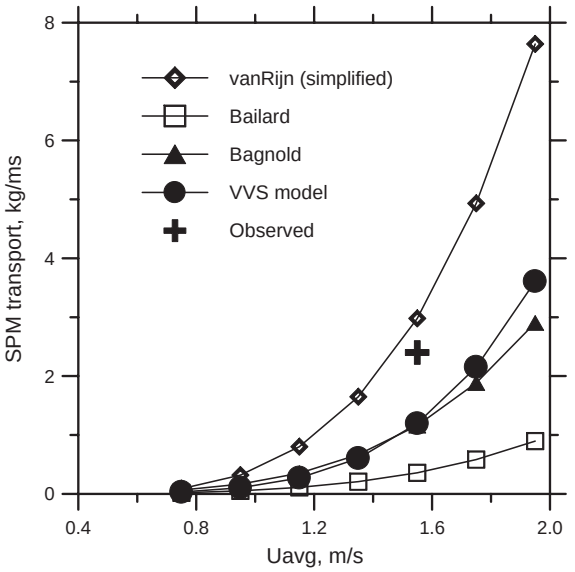

Fig. 2. SPM transport rates calculated with various models against observation taken in the Mississippi river (van Rijn, 1993), for the following parameters: $H = 12.05$ m, $U_{avg} = 1.55$ m/s, $d_{35} = 350$ mkm, $d_{50} = 400$ mkm, $d_{90} = 1500$ mkm, sediment density $\rho = 2650$ kg/m^3, $z_0 = 0.007$ m, $w_s = 0.059$m/s.

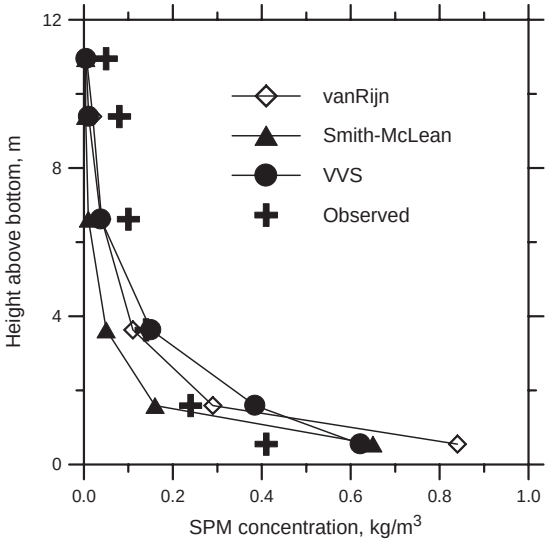

Fig. 3. Observed versus calculated SPM concentration profiles, the Mississippi river. Calculations using Smith-McLean and van Rijn methods were carried out by van Rijn (1993).

and from the Bailard formula

$$m = \frac{\varepsilon_s \rho_s \kappa^2 U_{\text{avg}}^3 \ln(a/z_0)}{g(s-1)w_s \ln^3(H/z_0 \text{e})}, \tag{36}$$

where a denotes the reference level, $a = 0.21$ m for the Mississippi case, see van Rijn (1993). The value of the efficiency factor for the VVS model was taken $\varepsilon_s = 0.082$, to match the observed value of the SPM load, $m = 1.73$ kg/m^2.

Fig. 3 shows the observed concentration profiles in the Mississippi river, calculated with the above parameters by van Rijn (1993, Section 7.4.3) and with the VVS model. Calculation with the VVS model gives the following flow parameters at $U_{avg} = 1.55$ m/s: the turbulent viscosity $K_z = 0.13$ m^2/s; Ekman depth $H_E = 60$ m; nepheloid layer thickness (e-fold) $h_d = 2.2$ m; a negligibly small SPM veering angle, $\alpha = 0.2°$. Figs. 2 and 3 show that, in the extreme case of shallow water the VVS model predicts the SPM transport rates and concentration profiles fairly close both to observations and predictions by the civil engineering models. It is particularly important that, over a range of flow parameters, the VVS model gives the transport rates close to that of van Rijn formula (Fig. 2) which, in turn, was validated and tuned against a large number of observations.

3.2. Simulations with the VVS model

The results of the previous section show that, in extreme cases of very deep or very shallow waters, the VVS model is consistent with the existing theories/observations. The results of model simulations in the intermediate range of parameters are discussed below. The angle of deviation of SPM transport from the surface current was calculated using Eq. (30) in a range of water depths $h = 5-50$ m and depth-averaged current speeds $U_{avg} = 0.1-1.2$ m/s.

Calculations were made for a steady uniform current over a flat bottom covered by medium/fine sediment (settling velocity $w_s = 0.001-0.02$ m/s). The Coriolis parameter and drag coefficient were taken as $f = 10^{-4}$ and $C_d = 2 \times 10^{-3}$ (Csanady, 1982, Section 1.6), respectively. Fig. 4 shows that, at a fixed bottom depth, the cross-current SPM transport decreases with an increase in current speed. This effect is due to the fact that stronger currents generate higher level of turbulence, and

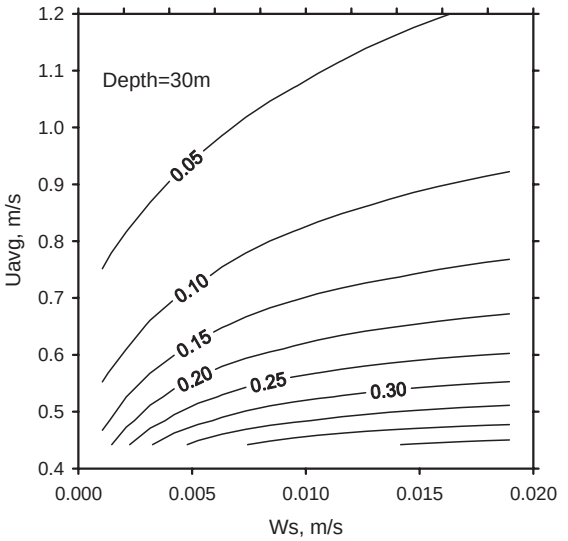

Fig. 4. Calculated ratio of cross-current to along-current SPM transport in 30 m of water for various flow speeds and sediment settling velocities, the VVS model.

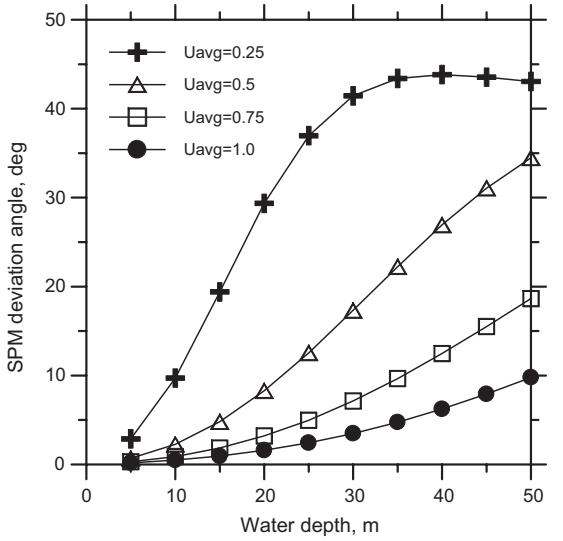

Fig 5. SPM transport deviation angle as a function of total water depth at the sediment settling velocity $w_s = 0.01$ m/s.

hence sediment particles are lifted higher within the water column, where the currents are more aligned with the surface current. Increased turbulence results also in a thickening of bottom Ekman layer. Thus, the near-bottom currents are more aligned with the direction of the surface current. The deviation angle depends also upon the sediment settling velocity and increases with the weight of suspended particles (Fig. 4). Heavier sediment is concentrated closer to the seabed, where deviation of the local current from the direction of that at the surface is the strongest.

Fig. 5 shows the angle of SPM veering from the direction of the surface current, as a function of total water depth and for a set of current velocities at $w_s = 0.01$ m/s. In shallower water (depth 5–10 m), velocity veering is negligible at speeds higher than 0.3–0.5 m/s. Within this depth range, the influence of the Earth's rotation can be ignored, so that both the velocity veering and traditional models (with no Coriolis effect involved) can be used. In water as deep as 20 m and more, the Coriolis effect turns the sediment flux by, typically, 10–30°. The effect is stronger in deeper waters and exhibits saturation, if the water depth exceeds about twice the Ekman scale. Coarse sediment (sand) has a very small *e*-folding length and hence it is affected by velocity veering at most. The angle between the surface current and the bottom shear stress gives a good estimate to the direction of both suspended and bedload transport. For finer sediments (e.g. medium/fine sand, silt) where the nepheloid layer height is significant, the veering angle is smaller, however it is more sensitive to the parameters of sediment and particularly to the settling velocity. Sediments of varying grain sizes occupy different parts of the Ekman spiral and generally move in different directions. Thus the velocity veering provides a mechanism for sorting sediments according to their grain sizes.

Another useful parameter, which is predicted by the model, is the thickness of the near-bottom nepheloid layer, h_c, see Eq. (19). Comparison with observations at $U_{\text{avg}} = 1.55$ m/s is shown in Fig. 3. Simulated values of h_c for a range of input parameters are given in Fig. 6. The thickness of the nepheloid layer increases as the current flows faster. The model also predicts a thicker nepheloid layer if the water is deeper. Both effects are due to the increase of turbulent diffusivity.

Correct parameterization of turbulence is crucial in determining the thicknesses of the Ekman layer, H_E, and the nepheloid layer, h_c. Agreement between the observed and simulated values (Figs. 2

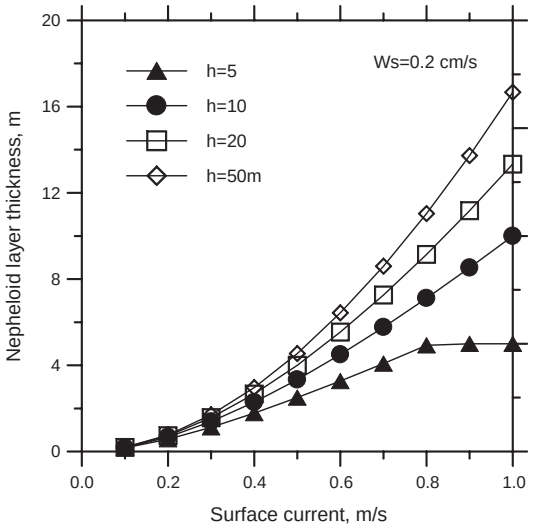

Fig. 6. Thickness of the near-bottom nepheloid layer for a steady current over flat bottom at $w_s = 0.01$ m/s.

and 3) proves that piecewise parameterization scheme used in the VVS gives realistic estimates of the main parameters and depth-integrated sediment transport rates. The accuracy of the vertical profiles of concentration are comparable with other algorithms, however this is where the limits of the present form of the VVS model lie. Better representation of the vertical profiles will need a more complex turbulent closure schemes. However the transport rates are more sensitive to the parameters of bottom sediments than to the vertical distribution of kinetic energy. The direction of sediment transport and hence the spatial structure of erosion and deposition are sensitive to the effect of velocity veering. This effect is missing in commonly used algorithms, see Soulsby (1997), but is represented in the VVS model.

4. Conclusions

Sediment transport in the marine environment is different from that in rivers and estuaries, in that the shelf seas are generally deep enough to accommodate the Ekman spiral or, at least, part of it. The Coriolis effect generates velocity veering in such a way that the current near the bottom flows at an angle to the current in the main body of water. As the suspended sediment transport occupies only lower part of the water column, than the direction of the (depth integrated) sediment transport is different from the direction of the (depth integrated) water flow. This effect is strongest for the coarse sediment and bedload transport. Fine sediments have a thicker nepheloid layer so that sediments move in different directions at different depth with the water column. Depth-integrated sediment transport in this case is less deviated from the free-stream water flow.

This paper presents a semi-analytical 2.5D model, which occupies a niche between 2DH models and fully 3D numerical models. The model resolves analytically the vertical structure of the SPM transport, whilst the horizontal variability and erosion/deposition fluxes are computed using numerical methods. This approach results in a fast numerical code, and the model algorithm is designed to be similar in format to the models used by civil engineers. Parameters of the bottom mixed layer, such as eddy viscosity and the thickness of the nepheloid layer, are produced by the model and are position-dependent. Model simulations show that effect of velocity veering can be significant, for both bedload and suspended load transports. The deviation angle between sediment transport and free-stream water flow is in the range of 5–30°, at typical shelf sea parameters. The model automatically reduces to traditional engineering style formulations in very shallow water, where velocity veering is of minor importance.

Acknowledgement

This work was partially funded by INTAS grant 01-460 Mass Transfer Through Submarine Canyons.

References

Alekseenko, S.V., Nakoriakov, V.E., Pokusaev, B.G., 1992. Undulated Flow of Liquid Films. Nauka Publishing, Novosibirsk, 255pp. (in Russian).

Barenblatt, G.I., Golitsin, G.S., 1973. Local Structure of Developed Dust Storms. MGU, Moscow, 44pp.

Bass, S.J., Aldridge, J.N., McCave, I.N., Vincent, C.E., 2002. Phase relationship between fine sediment suspension and tidal currents in the coastal seas. Journal of Geophysical Research 107, 3146.

Calvete, D., Walgreen, M., de Swart, H.E., Falques, A., 2001. A model for sand ridges on the shelf: effect of tidal and steady currents. Journal of Geophysical Research—Oceans 106, 9311–9325.

Coleman, G.N., Ferziger, J.H., Spalart, P.R., 1990. A numerical study of the turbulent Ekman layer. Journal of Fluid Mechanics 213, 313–348.

Csanady, G.T., 1982. Circulation in the Coastal Ocean. Reidel, Dordrecht, 279pp.

Davies, A.M., Jones, J.E., 1990. Application of a three-dimensional turbulence energy model to the determination of tidal currents on the northwest European shelf. Journal of Geophysical Research 95, 18143–18162.

Davies, A.M., Xing, J.X., 2001. Modelling processes influencing shelf edge currents, mixing, across shelf exchange, and sediment movement at the shelf edge. Dynamics of Atmospheres and Oceans 34, 291–326.

Davies, A.M., Xing, J., 2002. Processes influencing sediment movement on the Malin-Hebrides shelf. Continental Shelf Research 22, 2081–2113.

Dyer, K.R., 1986. Coastal and Estuarine Sediment Dynamics. Wiley, New York, 342pp.

Lentz, S.J., 1995. Sensitivity of the inner-shelf circulation to the form of the eddy viscosity profile. Journal of Physical Oceanography 25, 19–28.

Lentz, S.J., Trowbridge, J.H., 1991. The bottom boundary-layer over the northern California shelf. Journal of Physical Oceanography 21, 1186–1201.

McCandliss, R.R., Jones, S.E., Hearn, M., Latter, R., Jago, C.F., 2002. Dynamics of suspended particles in coastal waters (southern North Sea) during a spring bloom. Journal of Sea Research 47, 285–302.

McCave, I.N., 1972. Transport and escape of fine-grained sediment from shelf areas. In: Swift, D.J.P., Duane, D.B., Pilkey, O.H. (Eds.), Shelf Sediment Transport: Process and Pattern. Hutchinson and Ross, Dowden, pp. 225–244.

Monin, A.S., Yaglom, A.M., 1971. Statistical Fluid Mechanics. MIT Press, Cambridge, MA, 769p.

Niedoroda, A.W., Swift, D.J.P., 1991. Shoreface processes. In: Herbich, J.B. (Ed.), Handbook of Coastal and Ocean Engineering, Vol. 2. Gulf Publ. Co., Houston, pp. 735–770.

Pond, S., Pickard, G.L., 2001. Introductory Dynamical Oceanography, 2nd Edition. Butterworth-Heinemann, Oxford, 329pp.

Proctor, R., Holt, J.T., Balson, P.S., 2001. Sediment deposition in offshore deeps of the western North Sea: questions for models. Estuarine Coastal and Shelf Science 53, 553–567.

Ramp, S.R., Abbott, C.L., 1998. The vertical structure of currents over the Continental Shelf off Point Sur, CA, during Spring 1990. Deep-Sea Research II 45, 1443–1470.

Schoonees, J.S., Theron, A.K., 1995. Evaluation of 10 cross-shore sediment transport morphological models. Coastal Engineering 25, 1–41.

Shapiro, G.I., Akivis, T.M., Pykhov, N.V., Antsyferov, S.M., 2000. Transport of fine sediment with mesoscale currents in the shelf-slope zone of the sea. Oceanology 40, 305–311.

Simpson, J.H., 1998. Tidal Processes in Shelf Seas. In: Brink, K.H., Robinson, A.R. (Eds.), The Sea, Vol. 10. Wiley, New York, pp. 113–149.

Sleath, J.F.A., 1984. Sea Bed Mechanics. Wiley, New York, 335pp.

Soulsby, R., 1997. Dynamics of Marine Sands. Thomas Telford Publications, London, 243pp.

Stacey, M.W., Pond, S., Leblond, P.H., 1986. A wind-forced Ekman-spiral as a good statistical fit to low-frequency currents in a coastal strait. Science 233, 470–472.

Teisson, C., 1997. A review of cohesive sediment transport models. In: Burt, N., Parker, R., Watts, J. (Eds.), Cohesive Sediments. Wiley, New York, pp. 367–381.

Tomczak, M., Hao, D.M., 1989. Observations of the time-dependent planetary boundary layer. Ocean Sciences Institute Report 38, the University of Sydney, see also http://www.es.flinders.edu.au/~mattom/ShelfCoast/notes/chapter03.html.

van der Molen, J., 2002. The influence of tides, wind and waves on the net sand transport in the North Sea. Continental Shelf Research 22 (18–19), 2739–2762.

van Rijn, L.C., 1993. Principles of Sediment Transport in Rivers, Estuaries and Coastal Seas. Aqua publications, Amsterdam, 681pp.

Xu, Z.G., 1995. A transport approach to the convolution method for numerical modeling of linearized 3D circulation in shallow seas. International Journal for Numerical Methods in Fluids 20, 363–391.